Integrated Micro-Electro-Mechanical Sensor Development for Inertial Applications

J. J. Allen, R. D. Kinney, J. Sarsfield, M. R. Daily, J. R. Ellis, J.H. Smith, S. Montague
Sandia National Laboratories
Albuquerque, NM, 87185

R. T. Howe, B. E. Boser, R. Horowitz, and A. P. Pisano
Berkeley Sensor Actuator Center
University of California
Berkeley, CA, 94720

M. A. Lemkin, W. A. Clark, T. Juneau,
Integrated Micro Instruments
Berkeley, CA, 94704

Abstract

Electronic sensing circuitry and micro-electro-mechanical sense elements can be integrated to produce inertial instruments for applications unheard of a few years ago. This paper will describe the Sandia M^{3}EMS fabrication process, inertial instruments that have been fabricated, and the results of initial characterization tests of micro-machined accelerometers.

Introduction

Monolithically integrated micro-mechanical/micro-electronic systems have produced accelerometers for automotive applications. As integrated MEMS/CMOS fabrication processes such as those developed by U.C. Berkeley, Analog Devices, and Sandia Labs mature, additional systems for more sensitive inertial measurements will be developed. For example, the development of a very small, lightweight, inexpensive, and rugged Inertial Measurement Unit (IMU) would enable the widespread use of GPS-Aided Inertial Navigation Systems, which would be useful in commercial as well as military applications. Monolithically integrated silicon micro-electro-mechanical systems are an extremely promising technology and have the potential to achieve these IMU goals.

A collaboration of Sandia National Laboratories and the Berkeley Sensor Actuator Center (BSAC) at the University of California at Berkeley is pursuing the development of inertial devices to achieve the performance necessary for GPS-Aided Inertial Navigation Systems. Sandia and BSAC have designed and fabricated an Integrated Micro-Electro-Mechanical (IMEM) IMU shown in Figure 1. Although the ultimate goal of this effort is to develop a IMEM tactical grade inertial measurement unit fabricated in the M^{3}EMS process, which can be used in defense applications, there are ranges of other applications in which IMEM IMUs of lower quality can be used. Currently, there are activities underway to design, fabricate and experimentally characterize the performance of these devices. Simulation and modeling efforts are also being pursued to guide the design and modifications of the inertial devices, as well as determine the capabilities of an inertial system incorporating these devices.

This paper will discuss the following items:

- Sandia M^{3}EMS process which was used for fabrication of the inertial devices.
- The inertial devices that have been fabricated.
- Experimental characterization of the accelerometers.

DISCLAIMER

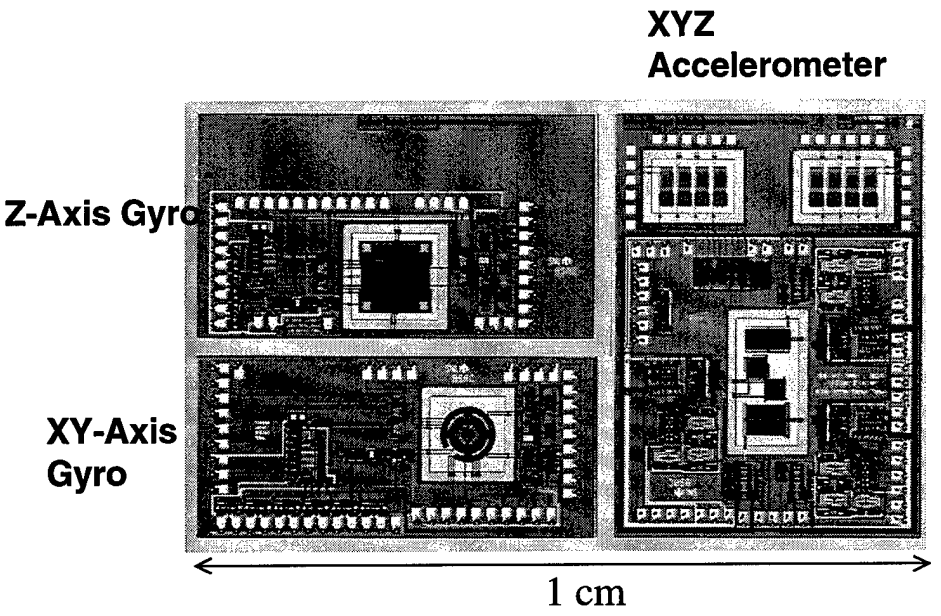

Figure 1. Six Degree of Freedom Inertial Measurement Unit fabricated with the Sandia M^{3}EMS process.

INTEGRATION OF MEMS AND MICROELECTRONICS

Recently, a great deal of interest has developed in manufacturing processes that allow the monolithic integration of Micro-Electro-Mechanical Systems (MEMS) with driving, controlling, and signal processing electronics. This integration promises to improve the performance of micromechanical devices as well as the cost of manufacturing, packaging, and instrumenting these devices by combining the micromechanical devices with an electronic sub-system in the same manufacturing and packaging process.

Several fabrication approaches [1,2] have been evaluated for the integration of CMOS and MEMS processes. The Sandia Modular, Monolithic, Micro-Electro-Mechanical Systems Technology (M^{3}EMS) is a modular MEMS approach to this integration. This process places the micromechanical devices in a shallow trench, planarizes the wafer, and seals the micromechanical devices in the trench. These wafers with the completed, planarized micromechanical devices are then used as starting material for a conventional CMOS process. This technique is equally applicable to other microelectronic device technologies such as bipolar or BiCMOS. In the Sandia facility, both 2 μm and 0.5 μm CMOS technologies on 6 inch wafers are available; the 2 μm process is being used as the development vehicle for the integrated technology. Since this integration approach does not modify the CMOS processing flow, the wafers with the subsurface micromechanical devices can also be sent to a foundry for microelectronic processing. Furthermore, the topography of multiple polysilicon layers does not complicate subsequent photolithography. A high-temperature anneal is performed after the devices are embedded in the trench prior to microelectronics processing. This anneal stress-relieves the micromechanical polysilicon and ensures that the subsequent thermal budget of the microelectronic processing does not affect the mechanical properties of the polysilicon structures. This anneal can affect the doping profile of commonly used epitaxial starting material; however, this effect can be easily addressed by increasing the epitaxial layer thickness of the starting material.

SANDIA M^{3}EMS PROCESS

This process has been described previously in more detail [3]. Figure 2 is a schematic cross-section of the integrated technology. First, alignment marks are etched onto the surface of wafer in order to provide reference locations for subsequent processing. A shallow trench (~ 6 μm for the single-level polysilicon structures

described here) is etched in (100) silicon wafers using an anisotropic etchant. The alignment marks from the top surface of the wafer are used as references to generate another set of alignment marks on the bottom surface of the trench.

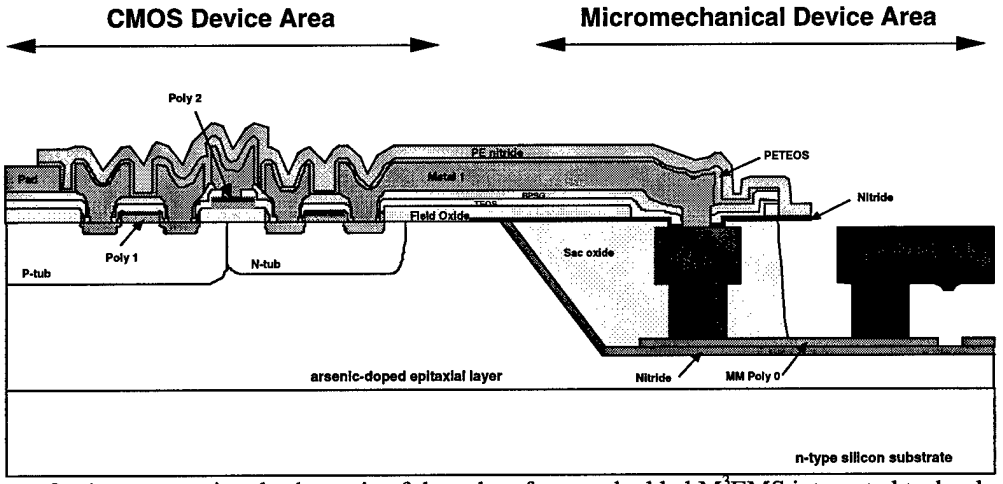

Figure 2. A cross-sectional schematic of the subsurface, embedded M^{3}EMS integrated technology.

A silicon nitride film is deposited to form a dielectric layer on the bottom of the trench. Multiple layers of polysilicon and sacrificial oxide and are then deposited and patterned in a standard surface micro-machining process. Polysilicon studs provide contact between the micromechanical devices and the CMOS; the depth of the trench is sized so that the top of the polysilicon stud lies just below the top of the trench. The shallow trenches are then filled with a series of oxide depositions optimized to eliminate void formation in high-aspect-ratio structures. The wafer is subsequently planarized with chemical-mechanical polishing (CMP). The entire structure is annealed to relieve stress in the structural polysilicon and sealed with a silicon nitride cap. At this point, conventional CMOS processing is performed. The backend of the process requires additional masks to open the nitride cap over the micromechanical layer prior to release of the micromechanical structures.

This integration process is not limited to the single-level polysilicon process described here. This process can be used with more intricate micromechanical processes such as the three-level polysilicon technology previously developed at Sandia [4].

FABRICATED INERTIAL SENSORS

The six degree of freedom inertial measurement unit, Figure 1, which was fabricated with the Sandia M^{3}EMS process consists of three accelerometers [5], dual-axis (in-plane) rate gyro [6], and a Z-axis (out-of-plane) rate gyro [7]. The fabrication process for this six degree of freedom Inertial measurement unit eliminates the need to manually align and assemble the individual sensors. This approach also provides on-chip A/D conversion circuitry, and enhanced sensitivity. Additional micro-machined inertial components have also been built in the Sandia technology such as the resonant accelerometers [8] and high-shock accelerometers [9].

Preliminary characterization of the accelerometers has been reported by Lemkin [5]. This +/- 25g accelerometer demonstrated an in-plane axis rms noise floor of 110 $\mu g/\sqrt{Hz}$ and an 84dB dynamic range at 100 Hz bandwidth. This performance significantly expands the number of applications for surface micro-machined accelerometers, but require further improvement in order to meet additional application requirements. For surface micro-machined inertial instruments to be qualified for use as navigational instruments much more extensive characterization of the instruments must be performed.

Accelerometer Characterization:

The X (in-plane) and Z(out-of-plane) accelerometers were tested using the procedures specified in IEEE STD 337-1972 [10]and IEEE STD 530-1978 [11]. The test uses the Earth's gravitation field as input to the accelerometer. Data is collected for different orientations of the

input axis relative to the local gravity vector. The test data is then used to develop a model of the accelerometer which includes bias, scale factor, non-linearity, cross-axis sensitivity, and temperature effects. The coefficients of the model are determined by regression analysis. The magnitude of the coefficients provides insight into the error sources present in the design. Stability of the coefficients over time and temperature provides a measure of device stability. The objectives of testing the accelerometers were to establish:

1. Baseline data on the performance of the first devices designed for fabrication in Sandia's M^3EMS process.
2. A robust infrastructure for supporting future tests of micro-machined inertial instruments.
3. Insight to guide future design efforts

Test Setup

A two-axis inertial test table manufactured by Contraves was used to orient the input axes of the three-axis accelerometer package relative to the local gravity vector. The test table has been carefully leveled relative to the local gravity vector. The table is equipped with a chamber capable of maintaining the temperature to within ±0.5 °C. Figure 3a shows the test table with the temperature chamber opened and the test board mounted on the table. Figure 3b also shows a schematic depicting the orientation of the table's inner gimbal and the test accelerometer axes for a typical test configuration. The input axes of the accelerometer are oriented to lie in the plane of the local gravity vector by a combination of table orientations and mounting of the accelerometer package on the table's inner gimbal. The table gimbals can be positioned with an accuracy of a few arcseconds of angle.

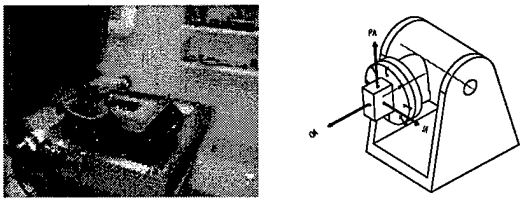

(a) (b)

Figure 3. Two Axis Inertial Test Table

The accelerometer test die was packaged in a 48 pin dual-in-line package. At this point in the development, no special effort was made to align the sensor input axes with axes of the package and the package was not hermetically sealed. The electrical output of an accelerometer channel is a pulse train in which the acceleration measurement is contained in the pulse density of the output pulses. The scale factor or quantity of output pulses per unit acceleration input is a function of the device clock frequency, which was 4MHz. Maintaining good clock stability is essential for achieving good accelerometer stability. This issue was addressed by clocking the accelerometer with a low drift, (±100 ppm from -10 to +70 °C) crystal oscillator. To accurately measure the power consumption of the accelerometer chip, circuitry was incorporated on the test board to measure the current flowing directly into the power supply pins of the test chip. Knowledge of the accelerometer temperature during testing is an essential parameter for characterizing the accelerometers stability over temperature. The chip was not directly accessible. Therefore, its package temperature was the parameter measured and used to determine temperature stability. A silicon temperature sensor, the AD590, was used to sense accelerometer package temperature.

The digitization scheme for the accelerometer channels is that of a ΔΣ converter. The acceleration information is contained in the density of its output pulse stream. Typically, in ΔΣ converters, this pulse stream is input to a finite impulse response (FIR) digital filter which is usually integrated with the converter's analog modulator. The digital filter's purpose is to (1) decimate the over-sampled analog modulator's output and (2) filter the high frequency noise to produce a lower frequency, high-resolution output. The test accelerometer contains only the analog modulator portion of a typical ΔΣ converter.

The digital filtering and decimation was accomplished in our test configuration by using a counter to effectively implement an averaging digital filter. That is, accumulating pulses over a known period and dividing by the period length provides an average frequency or ones density over the sample period. This average frequency is a measure of the input acceleration. For an accumulation period of 10 seconds, the filter bandwidth is 0.04Hz. The test data obtained is effectively high resolution DC data. Most of the noise content of the output pulse steam has been eliminated by the filtering action of our pulse accumulator filter.

Error Model

The error model used to describe the observed behavior of the accelerometer under the conditions described in the previous section is patterned after the model described in references 1 and 2. The physical source of the errors described in these references remain valid for the surface micro-machined accelerometer. In addition, there may be important error sources unique to the micro-machined accelerometer that are insignificant in larger scale device such as those for which the IEEE standards were addressing. These were not considered in this test series. One parameter that is common in micro-machined and conventional accelerometers is temperature sensitivity. However, due to the small scale of the micro-machined device, temperature is expected to play a larger role.

The error model components selected for the micro-machined devices are:

1. bias or zero offset
2. scale factor or gain
3. non-linearity
4. input axis misalignment from the case reference axis about the output axis
5. cross-axis sensitivity for acceleration inputs along the input and pendulous axes
6. temperature

Misalignment of the input axis about the pendulous axis was not examined. The cross-axis sensitivity for acceleration inputs along the input and output axes also was not examined. Due to the non-pendulous design of the test accelerometer, it is reasonable to expect that both these errors and error term 5 above are insignificant. That is, because acceleration is sensed in the test devices by a translation of the proof mass rather than pivoting of the proof mass about an "output" axis, there is no mechanism to give rise to cross-axis sensitivity to the first order.

The equation relating average output frequency with the error model components is as follows:

$$F_{avg} = K_0 + K_1\cos(\theta) + K_2\cos(\theta)^2 + K_3\sin(\theta) + K_4\sin(2\theta) + K_5\Delta T \quad (1)$$

where,

F_{avg}– Average output Frequency
K_0 – Bias, Hz
K_1 – Scale Factor, Hz/g
K_2 – g^2 non-linearity, Hz/g^2
K_3 – Input-axis misalignment, Hz/g
K_4 – cross-axis sensitivity, Hz/g^2
K_5 – Temperature sensitivity, Hz/°C
ΔT – Temperature change from nominal

Test Data

The objectives of these initial tests of the accelerometers were to characterize the test devices under static conditions for linearity and stability of scale factor and bias over temperature and time. Each test sequence was begun by first soaking, unpowered, the accelerometer test chip at a specific temperature. Three temperatures, 15.6, 21.2, and 26.7 degrees Celsius, were used in this test sequence. Following a temperature soak of one hour, we applied power to the test device and accumulated data for ten seconds intervals at each of 36 orientations of the accelerometer input axis by incrementing the test table indexing head by 10 degrees to transition to the subsequent positions.

The value of the coefficients of the error model were established by linear regression. Figures 4 and 5 are examples of the data reduction as described in equation 1. It shows the measured data and the error model equation with "best fit" coefficients. Figure 5 was constructed by compensating the data using the error model and plotting the results as a function of actual input acceleration as determined by test table orientation.

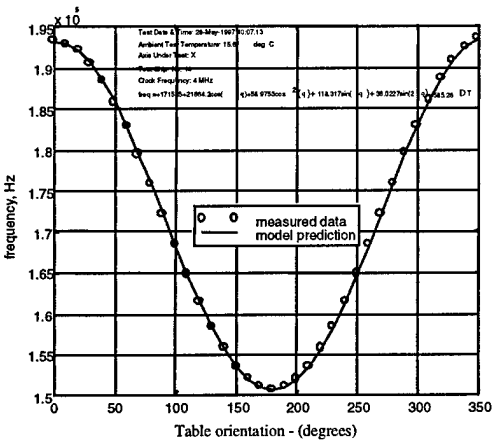

Figure 4. X Accelerometer Output versus Table Orientation

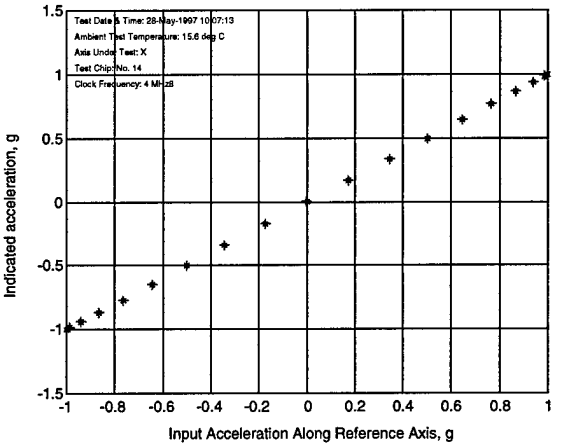

Figure 5. Indicated Acceleration (after compensation) versus Input Acceleration

Table 1. Model Coefficients for a X axis Accelerometer for Three Runs at 15.6 °C

	Run 1	Run 2	Run 3
Bias (Hz)	171548.6	171457.4	171244.9
Scale Factor, (Hz/g)	21655.35	21695.98	21926.83
G^2 Nonlinearity (Hz/g^2)	57.59382	66.77067	56.69872
Output Misalignment, (Hz/rad)	133.6652	154.3345	193.1641
Cross Axis Sensitivity (Hz/g^2)	33.41831	42.1883	84.36961
Temperature (Hz/°C)	531.2829	669.7465	1374.274

Table 2. Model Coefficients for a Z axis Accelerometer for Four Runs at 15.6 °C

	Run 1	Run 2	Run 3	Run 4
Bias (Hz)	244467.2	231510.8	230903.8	231846.1
Scale Factor, (Hz/g)	-21940.4	-15399.2	-14652.0	-15219.5
G^2 Nonlinearity (Hz/g^2)	-1695.21	127.8234	-35.3607	-83.946
Output Misalignment, (Hz/rad)	-3835.19	1352.309	74.62493	1064.03
Cross Axis Sensitivity (Hz/g^2)	-11320.7	72.2586	-28.0518	38.9159
Temperature (Hz/°C)	4080.815	5590.012	27.01001	4230.885

Stability over Temperature:

The test devices were tested at three temperatures, 15.6, 21.2, and 26.7 degrees Celsius. The important accelerometer parameters such as bias and scale factor were examined for changes. Over this small temperature range, the behavior is essentially linear. The error model coefficients were obtained for each data set and changes in bias and scale factor were calculated. The results were not distinguishable from the changes observed between data sets collected at the same ambient temperature. In future tests, larger temperature differentials will be explored

Short term Stability:

Short term stability in the context of this testing refers to the stability of accelerometer parameters between subsequent applications of power to the device. In other word, it refers to the stability of device parameters from turn-off to the next turn-on of the device for operation in the same environment. This stability is important for parameters such as bias because if the changes are random it is not possible to compensate for them. Tests were conducted wherein the input axis of the accelerometer was fixed in one orientation (typically at near zero g input) and the output of the device was measured by measuring the average frequency over a ten second interval for a period of five minutes or 30 samples. The interval between successive

applications of power was approximately one hour. Temperature at the accelerometer package was monitored as well. Figure 6 shows the behavior of the bias as function of time for three runs. The standard deviation of the first set of thirty samples is 7 milli-g, but the bias change in the absence of the initial transient is clearly more stable by about a factor of three.

The bias also possessed a long term drift as seen by observing the bias in terms of g presented in Table 2 versus the bias measured during the short term stability tests. The change from 7.9g of Table 2 to 10.7g of the stablility tests for this accelerometer occurred over a period of approximately one month. The z-axis accelerometer showed similar stability behavior.

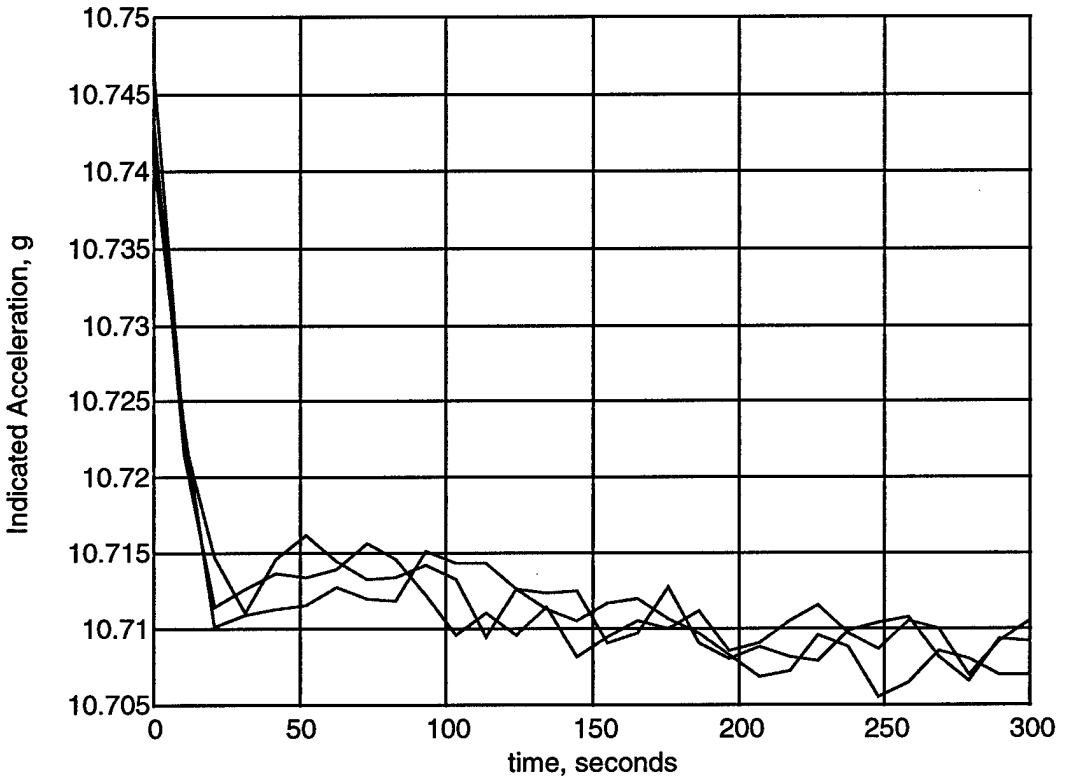

Figure 6. Stability of X Accelerometer Bias For Successive Power On Tests

Summary

This paper has described the Sandia M^3EMS fabrication process for integrated micro-machined inertial instruments. A 6-axis IMU consisting of 3 accelerometers and 3 axes of rate gyros have been fabricated. Initial characterization tests of the accelerometers have been performed. Additional characterization and redesign of the accelerometers are underway. Characterization of the gyro's will be performed in the near future.

The short-term stability of the X axis (in-plane) accelerometer was sufficiently adequate to allow consideration for use in medium performance inertial measurement systems. The Z axis (out-of-plane) accelerometer was not of the same performance class as the X axis accelerometer due to the nature of its design.

As expected the accelerometers possess considerable temperature sensitivity. The accelerometer measurements can be compensated for temperature sensitivity, however, the inclusion of a temperature sensor may be useful.

The prospect of achieving the low cost, low power, small size, and medium performance is highly probable for micro-machined accelerometers.

ACKNOWLEDGEMENTS

The process development engineers, operators, and technicians of Sandia's Microelectronics Development Laboratory should be acknowledged for their contributions to the process development and fabrication of these devices. Programmatic support from Michael Callahan of Weapon System 2010 and Tom Hitchcock of Joint DoD/DOE Munitions Technology is greatly appreciated. Sandia is a multi-program laboratory operated by Sandia Corporation, a Lockheed Martin Company, for the United States Department of Energy under contract DE-AC04-94AL85000.

Reference:

1. W. Kuehnel and S. Sherman, "A surface micromachined silicon accelerometer with on-chip detection circuitry," *Sensors and Actuators A*, vol. 45, no. 1, pp. 7-16, 1994.
2. W. Yun, R. Howe, and P. Gray, "Surface micromachined, digitally force-balanced accelerometer with integrated CMOS detection circuitry," *Proc. of the IEEE Solid-State Sensor and Actuator Workshop '92*, p. 126, 1992.
3. J. Smith, S. Montague, J. Sniegowski, J. Murray, and P. McWhorter, "Embedded micromechanical devices for the monolithic integration of MEMS with CMOS", *Proc. IEDM ' 95*, pp. 609-612, 1995.
4. J. Sniegowski and E. Garcia, "Microfabricated actuators and their application to optics," *SPIE* vol. 2383, pp. 46-64, 1995.
5. M. Lemkin, M. Ortiz, N. Wongkomet, B. Boser, and J. Smith, "A 3-axis surface micromachined sigma-delta accelerometer," *Proc. ISSCC '97*, pp. 202-203, 1997.
6. *Transducers '97*, Jun. 1997.
7. W. Clark, R. Howe, and R. Horowitz, "Z-axis vibratory rate gyroscope," *Micromachining Workshop III: Technology and Applications*, Sept. 1996.
8. T. Roessig, R. Howe, A. Pisano, and J. Smith, "Surface-micromachined resonant accelerometer," to be T. Juneau, et. al, "Dual axis operation of a micromachined rate gyroscope," to be presented at presented at *Transducers '97*, Jun. 1997.
9. B. Davies, C. Barron, S. Montague, J. Smith, J. Murray, T. Christenson, and V. Bateman, "High G MEMS Integrated Accelerometer," *Proc. SPIE Smart Electronics and MEMS*, Mar. 1997.
10. IEEE STD 337-1992. Standard Specification Format Guide and Test Procedure for Linear, Single-Axis, Pendulous, Analog, Torque Balance Accelerometer.
11. IEEE STD 530-1978. Standard Specification Format Guide and Test Procedure for Linear, Single-Axis, Digital, Torque Balance Accelerometer

Report Number (14) SAND--98-0574C
CONF-980420--

Publ. Date (11) 199804
Sponsor Code (18) DOE, XF
UC Category (19) UC-000, DOE/ER

DOE